

Hardware Description Document
Advanced Multi-Cell Lithium Battery Load Analyzer
2CE1EE



Jake Lin (CE)
Omar Mohamed (EE)
Tyler Shaw (CE)
Faculty Advisor: Scott Tierno

Contents

1.	Electromechanical Hardware	1
1.1.	Carbon Pile Load	1
1.2.	Shunt	3
1.3.	Analog Ammeter	6
1.4.	Fan	8
1.5.	Voltage Measuring Circuit	9
1.6.	Current Sensing Circuit	21
1.7.	Stepper Motor	27
2.	Local Interface Hardware	31
2.1.	Liquid Crystal Display (LCD)	31
2.2.	Pushbuttons	32
2.3.	Buzzer	34
3.	Remote Interface Hardware	35
3.1.	UART Bridge	35
4.	Other Hardware	38
4.1.	Microcontroller	38
4.2.	JTAG ICE Programmer	42
4.3.	Power Supply Board	45

Section 1 Electromechanical Hardware:

Section 1.1 Carbon Pile Load:

The carbon pile load acts as a variable resistor that is used to control the load current through the battery. A knob is used to move the carbon pile load, adjusting its resistance. Pictures of the carbon pile load are shown below in figures 1.1 and 1.2. A schematic of the carbon pile load is shown below in figure 1.3 (JL).

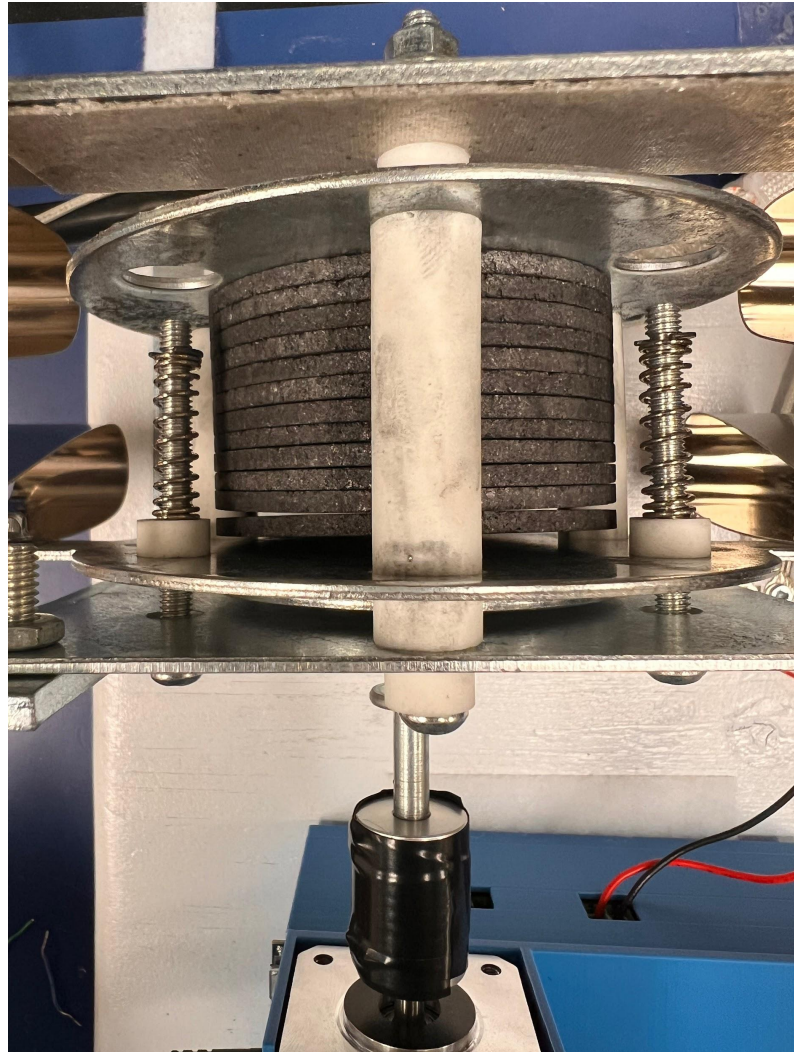


Figure 1.1: Carbon Pile Load Top View (JL)

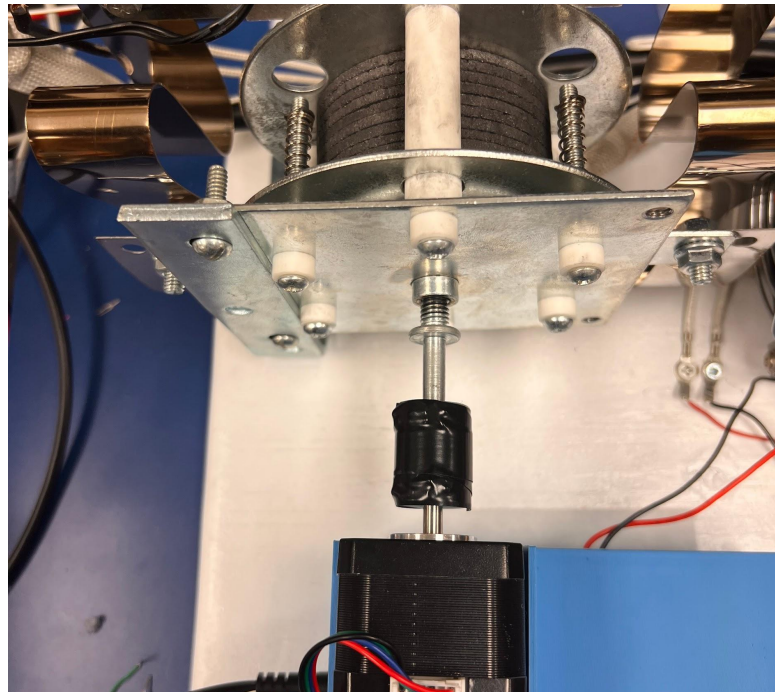


Figure 1.2: Carbon Pile Load Side View (JL)

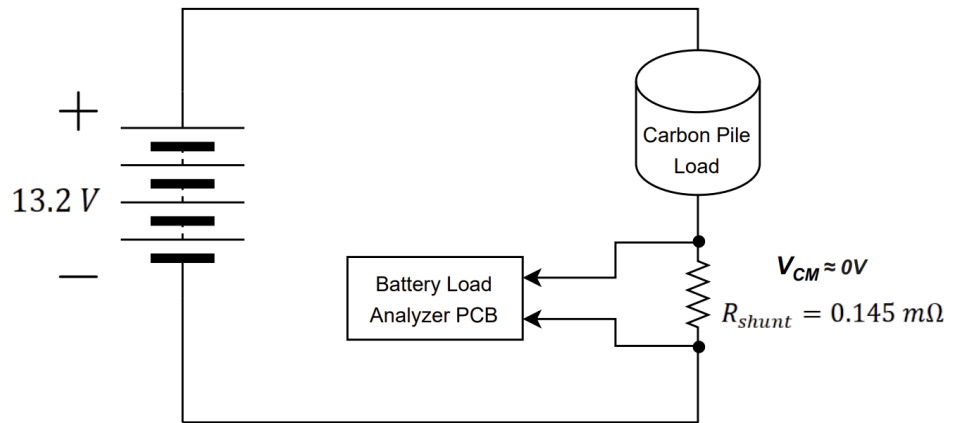


Figure 1.3: Carbon Pile Load Schematic (OM)

Section 1.2 Shunt:

The shunt will be used to measure the current being drawn by the battery and display it to the user so they know how much more to adjust the carbon pile. An image of the shunt is shown in figure 1.4. The red current sense wire is connected to the positive terminal of the shunt and black to the negative end. The benefit of placing the shunt at the negative end of the battery is so that the external op amp can process voltages close to 0V as opposed to 13V, and eliminating the need for a voltage divider to step down 13V, which would introduce additional inaccuracies (JL).



Figure 1.4: Shunt (JL)

To measure the current, the resistance of the shunt must be determined. These measurements are shown below in table 1.1. Using the measured voltage drop of the shunt and the current drawn from the circuit from the ammeter, the resistance is around 0.145 miliohm (JL).

Table 1.1: Shunt Resistance Measurements (JL)

Voltage Drop Over Shunt (V)	Current Measured by Ammeter (A)	Resistance (Ohms)
0.01454	100	0.000145437
0.02936	200	0.0001468
0.04367	300	0.0001455666667
0.05864	400	0.0001466
0.07264	500	0.00014529

When the shunt is placed in series with the carbon pile load, then the current that passes through the shunt is equal to the load current drawn by the carbon pile. This shunt resistance is small enough to not affect the load current being drawn and it will allow the team to measure the load current with the ADC by dividing the voltage across it by the known resistance in software. The shunt can be placed on the high-voltage side in between the carbon pile and the positive quad-pack terminal as shown in figure 1.5 or it can be placed on the low-voltage side in between the carbon pile and ground as shown in figure 1.6. For high-side current sensing, the common-mode voltage across the shunt is defined as the average of the voltages at the two terminals of the shunt resistor. Neglecting the small voltage drop across the shunt, this common-mode voltage is approximately equal to the quad-pack voltage of +13.2 V. Because the voltage drop across the shunt is minimal, both terminal voltages will be close to +13.2 V. Therefore, external voltage dividers are required to scale the voltage levels down to fall within the ADC's input range. To accurately amplify the small differential voltage across the shunt in the presence of a large common-mode voltage, an amplifier with a high common-mode rejection ratio (CMRR) is necessary (OM).

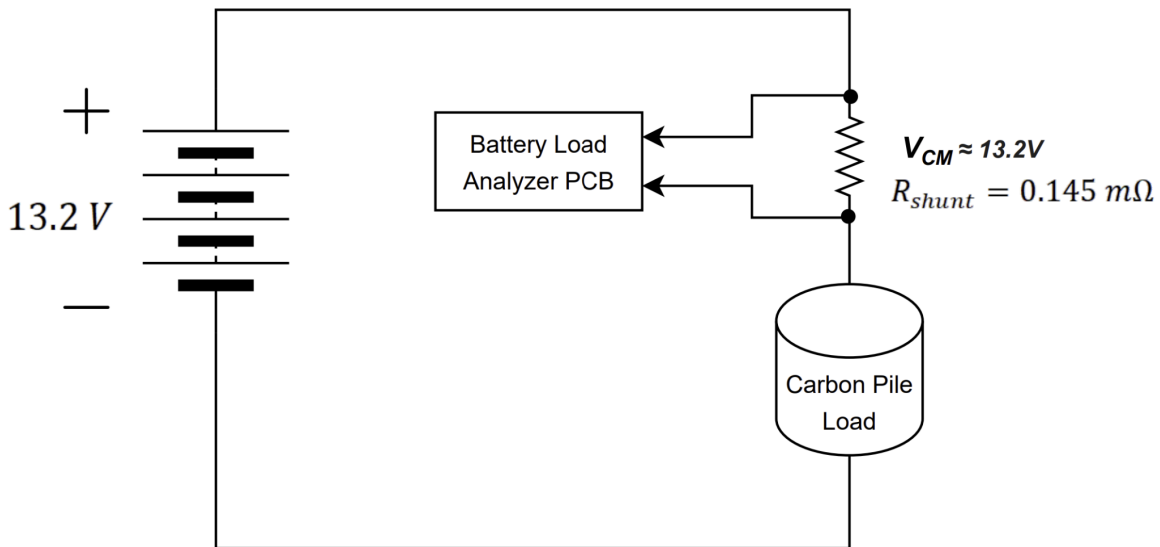


Figure 1.5: High-Side Current Sensing (OM)

In order to eliminate the need for external voltage dividers and a large CMRR, low-side current sensing can be used. Neglecting the small voltage drop across the shunt, this common-mode voltage is approximately equal to 0 V (ground). Because the voltage drop across the shunt is minimal, both terminal voltages will also be close to 0 V which is within the input range of the ADC (OM).

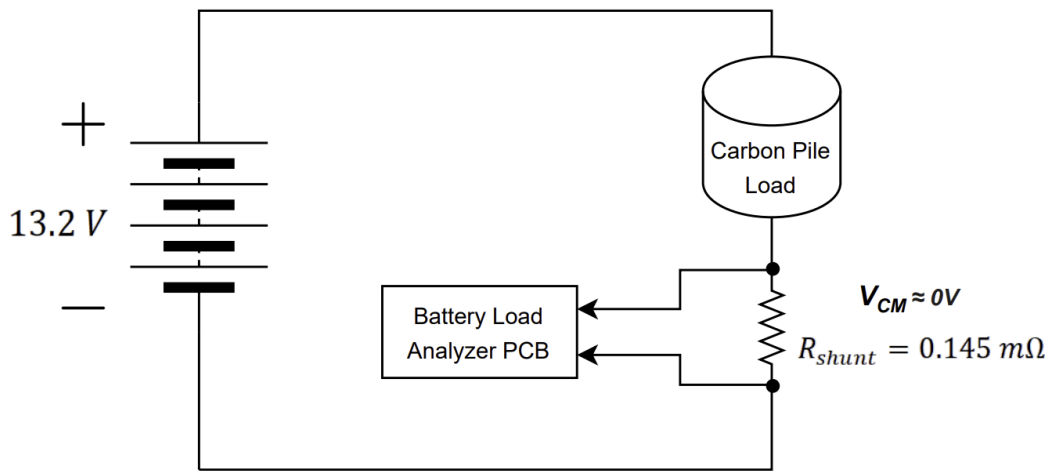


Figure 1.6: Low-Side Current Sensing (OM)

Section 1.3 Analog Ammeter:

In addition to digital current readings, the design also features an analog ammeter as shown in figure 1.7 below to display current measurements (TS).



Figure 1.7: Ammeter to Measure Current (TS)

The analog ammeter is connected in parallel with the shunt resistor, as shown in figure 1.8 below. Note that the battery load analyzer PCB is excluded from this figure (OM).

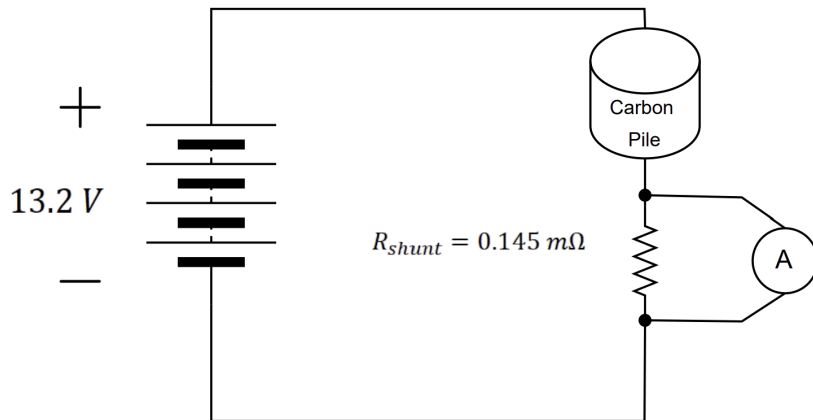


Figure 1.8: Analog Ammeter Connection (OM)

It draws a small amount of current from the voltage drop across the shunt resistor and generates a magnetic field. The magnetic field causes a mechanical deflection of the needle at an angle that is proportional to the current. The scale markings on the meter translate the needle's deflection angle into a current value in amperes. In order to calibrate the ammeter, a current limiting resistor is placed in series to fine tune the deflection angle of the needle until the current indicated by the scale markings exactly matches the current through the shunt. The calibration setup is shown in figure 1.9 below (OM).

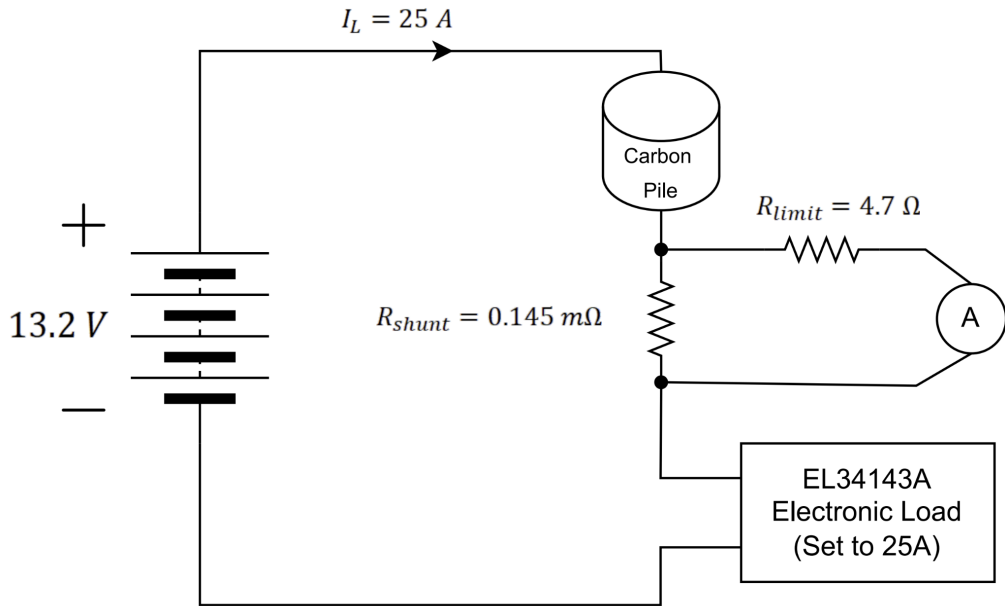


Figure 1.9: Analog Ammeter Calibration Setup (OM)

The EL34143A electronic load is connected in series with the quad-pack and is configured to set the current drawn from the quad-pack to exactly 25A. The current limiting resistor is adjusted until the current reading on the analog ammeter is exactly equal to 25A, which is the value set by the electronic load. Note that the carbon pile was fully compressed to act as a short-circuit during the calibration. After performing the calibration in the lab, the current limiting resistor value was determined to be 4.7Ω (OM).

Section 1.4 Fan:

The carbon pile becomes very hot easily when drawing a large amount of current. A fan is needed to cool down the carbon pile. An image of the fan is provided below as figure 1.10. The fan runs at 12 V. It is powered by the PCB power supply board. An image of the connection to the PCB is provided as in figure 1.11.



Figure 1.10: Fan (JL)



Figure 1.11: Fan Power Supply Connector on PCB (JL)

Section 1.5 Voltage Measuring Circuit:

To measure the voltages of each battery, a voltage divider is used. Connections to the battery and circuit are shown below in figures 1.12 and 1.13 respectively and the schematic is shown in figure 1.14. We chose alligator clips since it allowed us to break the circuit in the emergency that the stepper motor or carbon pile shaft got stuck during a loaded test. However this does have a drawback which is that the copper contacts of the clips will sometimes burn at currents near 300 A. Nevertheless, we recommend not drawing more than 250 A from the battery since the carbon pile gets exponentially harder to crank and one will risk getting the shaft stuck when loading beyond 250 A (JL).

- **Green wire** → Battery 1 positive terminal.
- **Yellow wire** → Battery 2 positive terminal.
- **White wire** → Battery 3 positive terminal.
- **Red alligator clip** → Red-marked square (Battery 4 positive terminal).
- **Black alligator clip** → Non-color-coded square (Ground/Negative terminal).

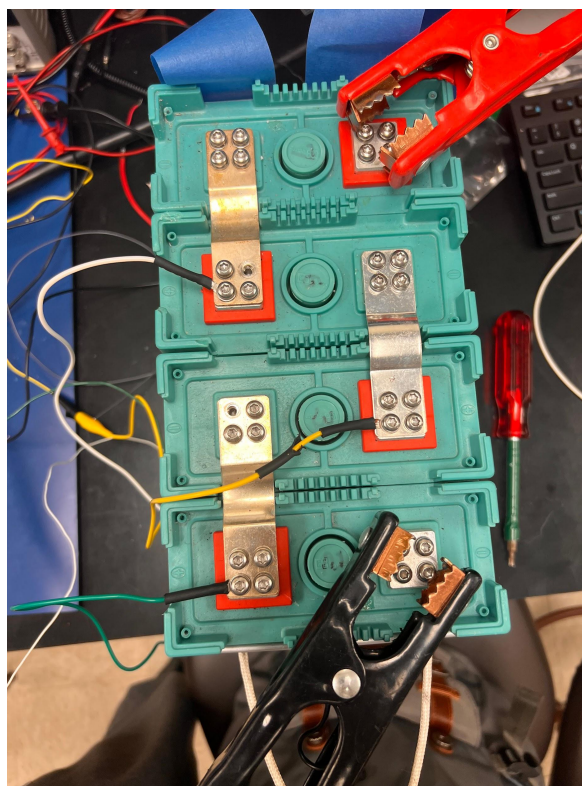


Figure 1.12: Voltage Divider Connections to Battery (JL)

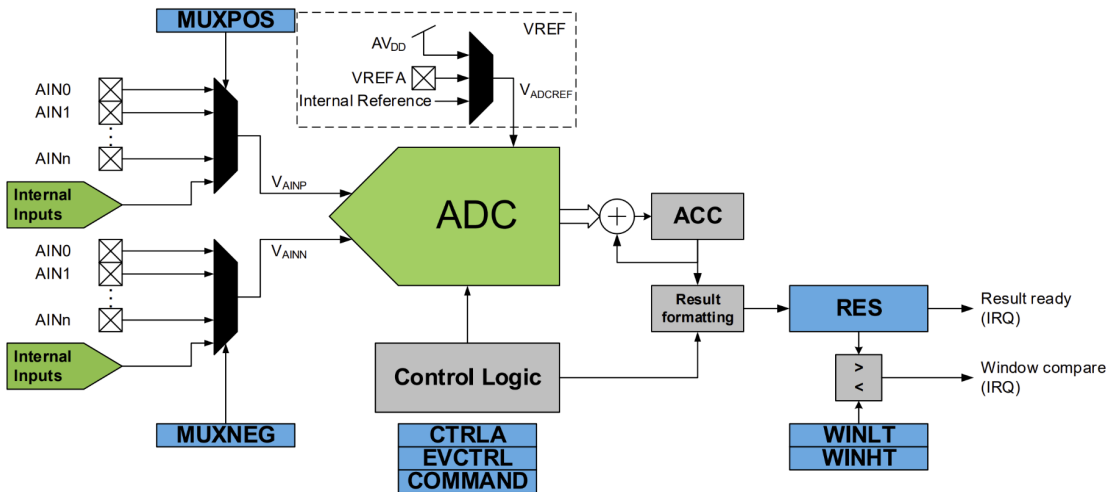


Figure 1.13: Voltage Divider Connections on PCB (JL)

The ADC will be used to measure the battery cell voltages and measure the voltage across the current sensing resistor. These are all differential measurements so either a differential ADC or a single-ended ADC with a front-end differential amplifier can be used. Additionally, the group must decide whether to use an ADC that is internal to our microcontroller or an external ADC integrated circuit. Since this project does not require a particularly high sample rate or resolution the group has decided to use the AVR128DB48's internal ADC because it requires less support circuitry and it can be configured to make either single-ended or differential measurements. The ADC of the AVR128DB48 has up to 22 different input channels that can be multiplexed using software commands. For this design, the group will select the ADC input pin using software rather than using an external analog multiplexing scheme. A block diagram of the internal ADC is shown below in figure 1.14 (OM).

33.2.1 Block Diagram

Figure 33-1. Block Diagram



33.2.2 Signal Description

Pin Name	Type	Description
AIN[n:0]	Analog input	Analog input to be converted
VREFA	Analog input	External voltage reference pin

Figure 1.14: AVR128DB48 ADC Peripheral Block Diagram (Datasheet Section 33.2.1)

The internal ADC of the AVR128DB48 can also be configured to have 12-bit or 10-bit resolution. If the ADC is configured to make differential measurements, the most-significant-bit (MSB) is used as a signed bit. Additionally, the reference voltage options of the ADC are shown below in figure 1.15 (OM).

Bits 2:0 – REFSEL[2:0] Reference Select

This bit field controls the reference voltage level for ADC0.

Value	Name	Description
0x0	1V024	Internal 1.024V reference ⁽¹⁾
0x1	2V048	Internal 2.048V reference ⁽¹⁾
0x2	4V096	Internal 4.096V reference ⁽¹⁾
0x3	2V500	Internal 2.500V reference ⁽¹⁾
0x4	-	Reserved
0x5	VDD	VDD as reference
0x6	VREFA	External reference from the VREFA pin
0x7	-	Reserved

Note:

1. The values given for internal references are only typical. Refer to the *Electrical Characteristics* section for further details.

Figure 1.15 - AVR128DB48 ADC0 Reference Voltages (Section 21.5.1 of Datasheet)

The reference voltages are generated from a bandgap reference which is stable over a wide range of operating conditions. A block diagram of the internal reference voltages is shown in figure 1.16 (OM).

21.2.1 Block Diagram

Figure 21-1. VREF Block Diagram

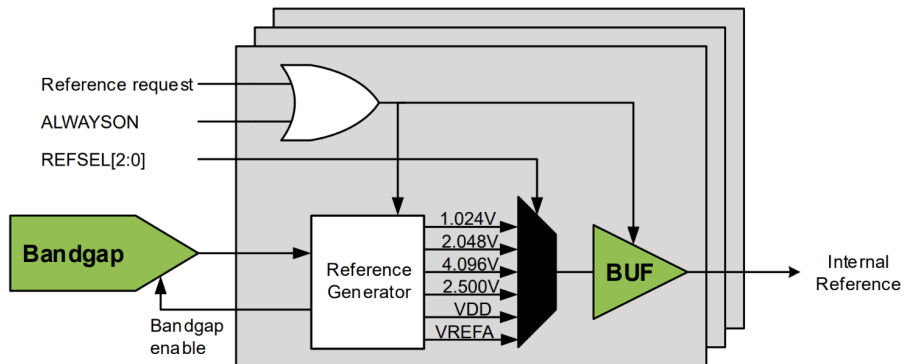


Figure 1.16: AVR128DB48 Analog Voltage References (Section 21.2.1 of Datasheet)

Additionally, the integer result of the ADC in various configuration modes is shown in figure 1.17. Resolution is defined as the smallest measurable voltage increment (quantization step). It is equal to the voltage corresponding to an integer result of 1 or one least-significant-bit (LSB) (OM).

33.3.3.5 Conversion Result (Output Formats)

The result of an analog-to-digital conversion is written to the 16-bit Result (ADCn.RES) register and is given by the following equations:

$$\text{Single-ended 12-bit conversion: } RES = \frac{V_{AINP}}{V_{ADCREF}} \times 4096 \in [0, 4095]$$

$$\text{Single-ended 10-bit conversion: } RES = \frac{V_{AINP}}{V_{ADCREF}} \times 1024 \in [0, 1023]$$

$$\text{Differential 12-bit conversion: } RES = \frac{V_{AINP} - V_{AINN}}{V_{ADCREF}} \times 2048 \in [-2048, 2047]$$

$$\text{Differential 10-bit conversion: } RES = \frac{V_{AINP} - V_{AINN}}{V_{ADCREF}} \times 512 \in [-512, 511]$$

Figure 1.17 - AVR128DB48 ADC Resolution (Section 33.3.3.5 of datasheet)

The equations below show that there is a clear tradeoff between resolution and input range when selecting the reference voltage. If the input range is defined as the difference between the minimum and maximum allowable inputs (single-ended or differential) and it is assumed that an LSB is negligible in comparison to the full scale value, the following relationships can be observed in equations 1 and 2 (OM).

$$RESOLUTION = \frac{V_{ADCREF}}{2^N} \quad (1)$$

$$INPUT\ RANGE \cong V_{ADCREF} \quad (2)$$

Note that the input is V_{AINP} for single-ended signals and $V_{AINP} - V_{AINN}$ for differential signals. Additionally, note that N is the number of bits and that a smaller resolution is more precise and has better accuracy. For a fixed number of bits, the input range is *proportional* to the reference voltage and the resolution (precision) is *inversely proportional* to the reference (OM).

Most of the battery terminal voltages are above the microcontroller power supply voltage, therefore, they must be attenuated as to fit within the input range of the ADC. Too much attenuation will reduce the input signal level and decrease the signal-to-noise ratio of our measurement. For this reason the group decided not to use the 1.024V reference as the input signal would require too much attenuation to fit within the ADC input range. After experimenting in the lab, the team found that the 2.048V reference gave the most accurate ADC measurements. The experimental results are shown below in table 1.2 (OM).

Table 1.2: Voltage Measurements Using Different ADC Reference Voltages (TS)

Battery Voltage from Multimeter (V)	Battery Voltage from MCU's ADC Using 2.048 V Voltage Reference (V)	Battery Voltage from MCU's ADC Using 3.3 V Voltage Reference (V)
3.32	3.307	3.307
3.34	3.350	3.355
3.33	3.328	3.334
3.32	3.307	3.313

In order to measure the voltage across each battery cell, the ADC is configured in differential mode and the resolution is chosen to be 12 bits. All of the battery cell voltages in this circuit are positive, therefore, the MSB (sign bit) will always be 0 because $V_{AINP} \geq V_{AINN}$. As a result, the resolution with respect to *positive* input signals where $V_{AINP} \geq V_{AINN}$ is effectively 11 bits, since the 12th bit will always be 0. Therefore, when the ADC is in differential mode, the effective voltage resolution of the ADC for *positive* input voltages will be 1 mV, as shown in equation 3 (OM).

$$RESOLUTION = V_{min} = \frac{V_{ADCREF}}{2^{11}} = \frac{2048 \text{ mV}}{2048} = \mathbf{1mV} \quad (3)$$

The total voltage across the battery pack is 13.2V and the microcontroller input pins have a maximum rated voltage of 3.6V when a 3.3V power supply is used. Additionally, as previously discussed, the ADC is configured in differential mode, therefore, all differential input voltages must be scaled to fit within the ADC input range for accurate measurements. If the differential input voltage exceeds the ADC reference voltage, then the result will be clipped at the full-scale value. For the faculty advisor's quad-packs, the nominal differential voltage across each battery cell is 3.3V, therefore, the minimum voltage divider ratio required to ensure the differential voltage is within the ADC input range is about 1.6 (OM).

$$\frac{V_{OUT}}{VIN} \geq \frac{3.3V}{2.048V} \cong 1.612 \quad (4)$$

However, the positive terminals of the battery cells are above the absolute maximum rating of 3.6V. In order to prevent damage to the microcontroller, a larger voltage divider ratio is required to scale the positive battery terminal voltage down to within the maximum rating of the microcontroller input pins. In order to simplify the software and hardware assembly, the group has decided to use the same voltage divider ratio for all of the battery cell measurements. The maximum voltage across the entire quadpack is 13.2V, therefore, the minimum voltage divider ratio to ensure that all microcontroller pin voltages remain within the maximum rating 3.6V is about 3.67

$$\frac{V_{OUT}}{VIN} \geq \frac{13.2V}{3.6V} \cong 3.67 \quad (5)$$

To provide an additional safety margin, a voltage divider ratio of 5.3 was chosen with the following resistor values.

$$R_1 = 1 \text{ k}\Omega \quad (6)$$

$$\frac{R_1}{R_1 + R_2} = 5.3 \rightarrow R_2 = 4.3 \text{ k}\Omega \quad (7)$$

The battery cell terminals are connected to the PCB with terminal blocks. A schematic of the voltage dividers used to scale the battery cell voltages to within the rated voltage levels is shown below in figure 1.18. Additionally, 100nF capacitors to ground are connected to each battery cell input in order to filter noise and prevent the voltages from dropping during the conversion process. During layout, the capacitors should be placed as close to the ADC as possible (OM).

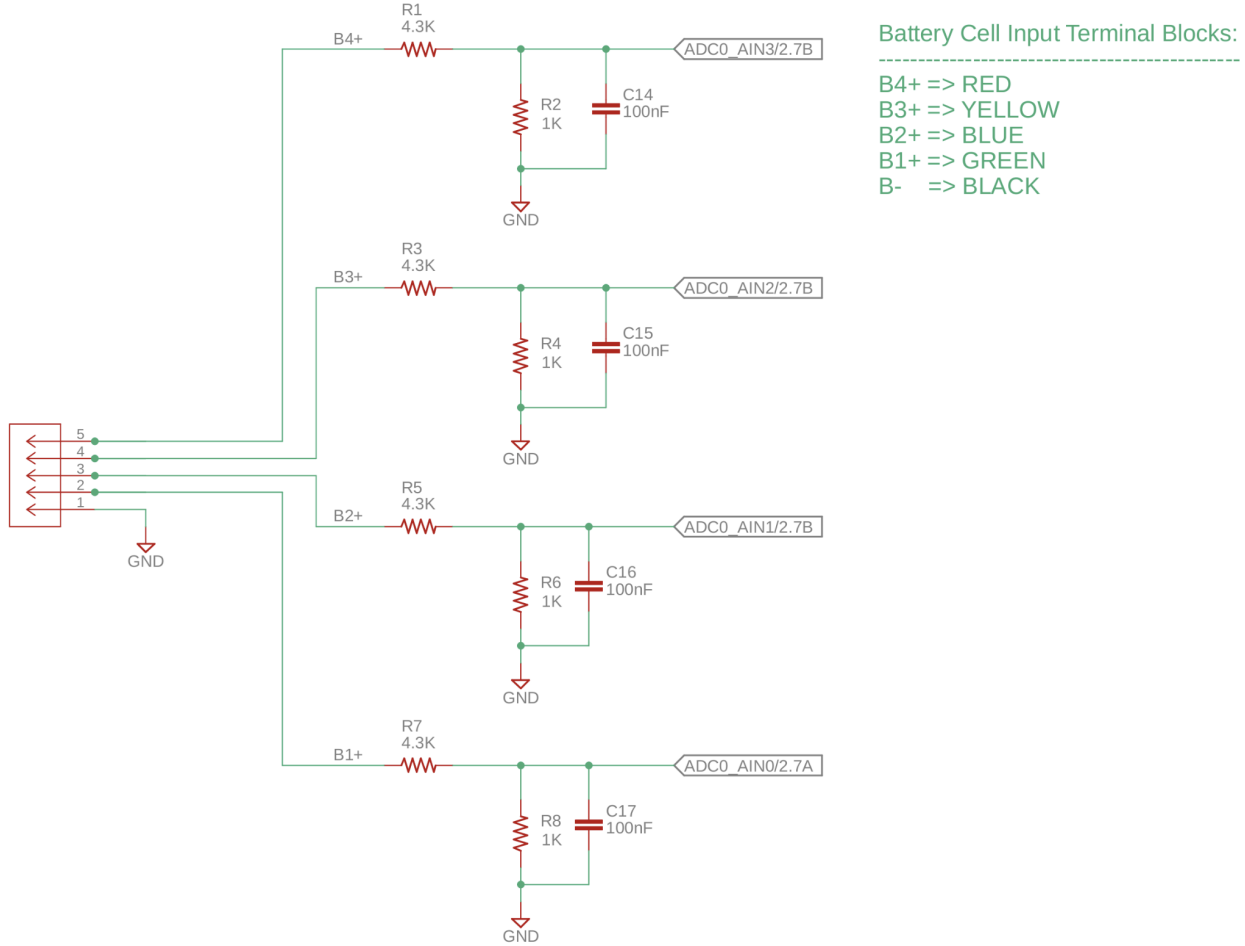


Figure 1.18: Input Voltage Dividers (OM)

Since all of the positive battery terminal voltages are divided by 5.3, the differential voltages are also divided by 5.3 due to the distributive property.

$$\left(\frac{V_2}{5.3} - \frac{V_1}{5.3} \right) = \frac{V_2 - V_1}{5.3} \quad (8)$$

As a result the input voltage of the ADC is divided by a factor of 5.3 and the voltage resolution for the differential battery cell measurements is 5.3 mV

$$V_{min} = \frac{V_{ADCREF}}{5.3 \times 2^{11}} = \frac{2048 \text{ mV}}{5.3 \times 2048} = 5.3 \text{ mV} \quad (9)$$

Note that inaccuracies can occur if the resistor values are not properly matched, therefore 1% tolerance resistors are used. This is because software multiplies the measured ADC input voltage

by the voltage division ratio to calculate the original value. If the resistors are different from their nominal value, then the actual voltage divider ratio will not be equal to the value written into software (OM).

Figure 1.19 shows the voltages measured by the MCU displayed on the LCD for a manual test performed with a load current of 100 A and figure 1.20 shows the voltages measured for an automated test performed with a load current of 100 A. The unloaded voltages are shown in the left column and the loaded voltages in the right column. The battery cells are labeled from top to bottom in ascending order, for example, “B1” corresponds to the bottom battery cell in the quad-pack with a nominal positive terminal voltage of 3.3V and “B4” corresponds to top battery cell in the quad-pack with a nominal positive terminal voltage of 13.2 V (TS).

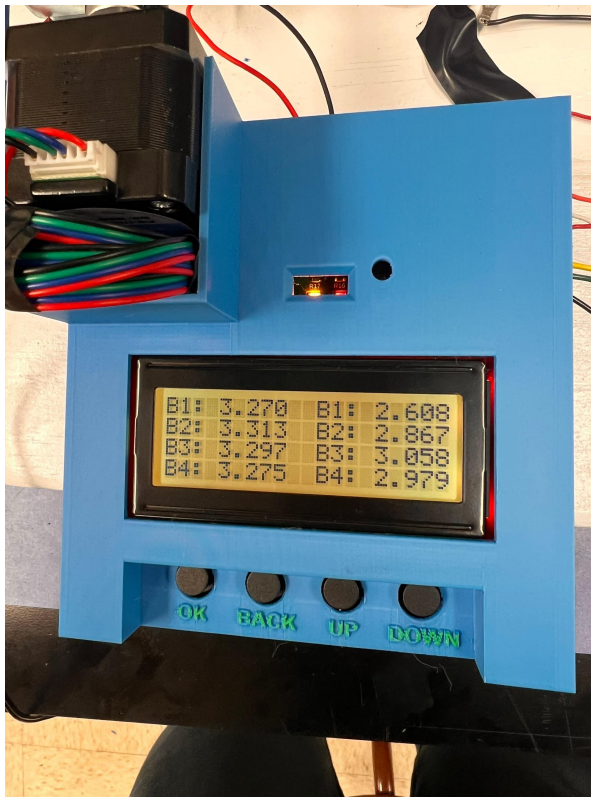


Figure 1.19: Measured Unloaded and Loaded Voltages for Manual Test (JL)



Figure 1.20: Measured Unloaded and Loaded Voltages for Automated Test (JL)

Tables 1.3 and 1.4 compare the unloaded voltages measured by the MCU with the voltages measured by a multimeter during a manual and automated test respectively (JL).

Table 1.3: Comparison of the MCU and Multimeter Measured Voltages for Manual Test (JL)

Battery Voltage from MCU's ADC Using 2.048 V Voltage Reference (V)	Battery Voltage from Multimeter (V)
3.270	3.300
3.313	3.290
3.297	3.300
3.275	3.290

Table 1.4: Comparison of the MCU and Multimeter Measured Voltages for Automated Test (JL)

Battery Voltage from MCU's ADC (V)	Battery Voltage from Multimeter (V)
3.270	3.300
3.313	3.290
3.297	3.300
3.275	3.290

The unloaded voltages are generally accurate within about 0.03 V, which is slightly higher than what the faculty advisor originally asked for. The reason for this discrepancy in voltage is because the accuracy of the microcontroller's ADC is limited in precision to 5mV when the external voltage dividers are used. Additionally, the microcontroller ADC is not ideal and there is a non-deterministic error between the voltage measured by the ADC and the actual input voltage. Table 1.5 compares the voltages measured by the ADC with the input voltage measured using a multimeter. This is the voltage of the battery cell after it has been stepped down by a factor of 5.3 from the voltage divider network (OM).

Table 1.5: Comparison of Input Voltage and Voltage Measured by ADC (JL)

ADC Input Voltage (V)	Voltage Measured by ADC (V)
0.617	0.620
1.242	1.244
1.864	1.865
2.482	2.482

The voltage reference could be decreased to increase precision, but then the input range would be reduced and the current reading would not be able to reach 500A since the full-scale voltage would be decreased. As a result, the voltage reference could not be decreased further than 2.048 V (TS).

Another source of error is that the resistor values used to create the voltage dividers are not exact, even though 1% tolerance resistors were used. Therefore, when software calculates the battery voltages based on the ADC value, the voltage divider ratio may not be exactly 5.3. Table 1.6 shows the input and output voltages for the voltage dividers used to scale down each battery cell voltage (OM).

Table 1.6: Voltage Divider Ratios (JL)

Voltage Divider Input (V)	Voltage Divider Output (V)	Voltage Divider Ratio (V/V)
3.280	0.620	5.290
6.580	1.244	5.289
9.870	1.865	5.292
13.17	2.482	5.306

Another source of error is thermal noise due to the resistors used in the voltage dividers. Any current that passes through the resistors, causes the physical matter to undergo molecular vibrations as a result of the thermal energy. The raw ADC measurements are accurate to within the theoretical 5mV and the voltage divider ratios are very close to the nominal values. As a result, it appears that the main source of battery voltage measurement inaccuracy is thermal noise generated by the resistive voltage dividers. The equivalent noise voltage caused by the thermal noise of each resistor is given by the following equation (OM).

$$e_{nR} = \sqrt{4KTBR_0} \quad (10)$$

Section 1.5 Current Sensing Circuit:

As mentioned earlier, the voltage drop across the shunt will be used to determine the load current. However, since the shunt produces very small voltages, the voltages need to be amplified by an op amp so they can be read by the microcontroller. An image of the op amp and current sense wires is shown below in figure 1.21 and 1.22 respectively (JL).



Figure 1.21: Op Amp on PCB (JL)

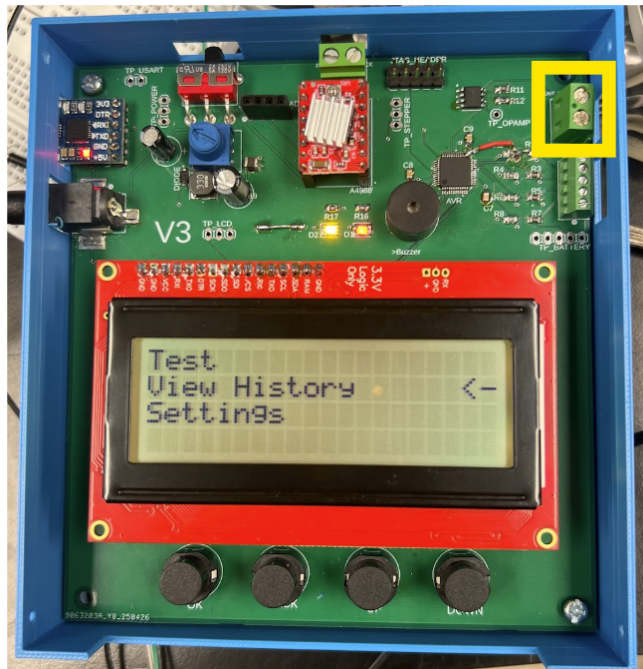


Figure 1.22: Current Sense Wires on PCB (JL)

If no amplification is used and a differential ADC measurement is made directly on the voltage drop across the shunt, then the smallest measurable current increment (current resolution) is

$$I_{min} = \frac{V_{min}}{R_{shunt}} = \frac{1 \text{ mV}}{0.183 \text{ m}\Omega} \cong \mathbf{5.46 A} \quad (11)$$

Additionally, if we assume that the minimum current is negligible in comparison to the full-scale current, then the maximum measurable current is

$$I_{max} \cong \frac{V_{ADCREF}}{R_{shunt}} = \frac{2048 \text{ mV}}{0.183 \text{ m}\Omega} \cong \mathbf{11,191 A} \quad (12)$$

If the input current range is between 0A and 11,191A then the resolution expressed as a percent of the maximum allowable input is about 0.05%

$$I_{res} = \frac{I_{min}}{I_{max}} = \frac{5.46}{11,191} \cong \mathbf{0.0488\%} \quad (13)$$

For our application, the current is limited to between 0A and 500A, therefore, the resolution as a percentage of the full-scale value is about 1.1%.

$$I_{res} = \frac{I_{min}}{I_{max}} = \frac{5.46}{500} \cong \mathbf{1.092\%} \quad (14)$$

It is now clear that without amplification, less than 5% of the available ADC resolution would be used if the current is limited to between 0 and 500A. In order to make effective use of the ADC's input range and increase measurement precision, a differential amplifier must be used to amplify the voltage drop before it is measured by the ADC. The group has decided to use the AD8410A current sense amplifier in the configuration shown in figure 1.23 (OM).

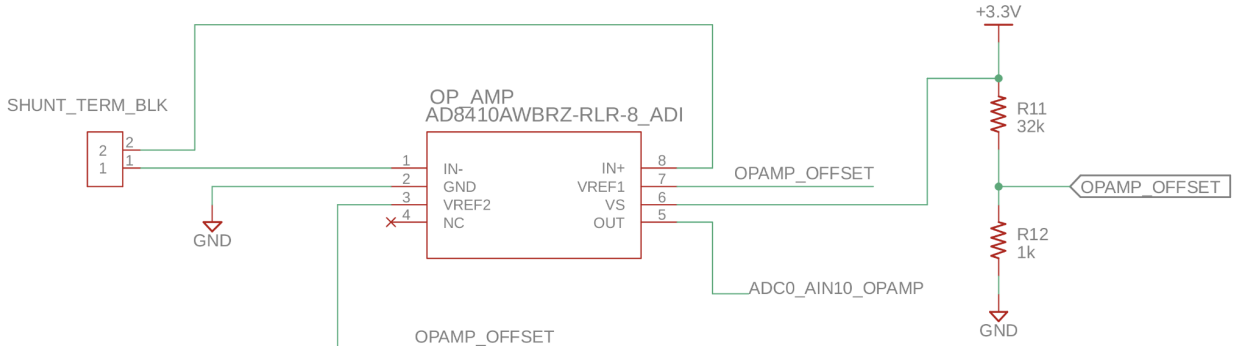


Figure 1.23: AD8410A Current Sense Schematic (OM)

The AD8410A is a differential-input, single-ended-output current sense amplifier with a fixed differential voltage gain of 20 V/V. After experimenting with the amplifier, the group found that the output voltage could not go below 3 mV even with 0 A of current passing through the shunt. This resulted in a nonzero current being measured even when the load current through the shunt was 0 A. Figure 1.24 shows how an external voltage source can be used to add a reference offset to the output of the AD8410A (OM).

External Referenced Output

Tie V_{REF1} and V_{REF2} together and to a reference to produce an output equal to the reference voltage when there is no differential input (see [Figure 53](#)). The output decreases with respect to the reference voltage when the input is negative, relative to the $-IN$ pin, and increases when the input is positive, relative to the $-IN$ pin.

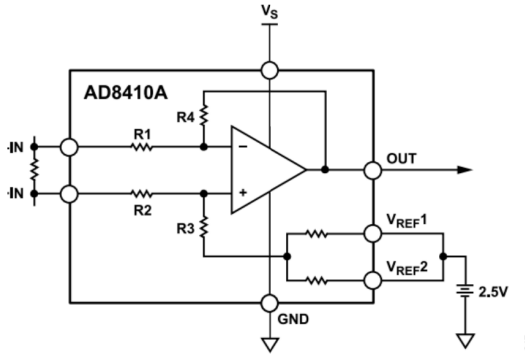


Figure 53. External Referenced Output

Figure 1.24: AD8410A External Reference Output (Datasheet page 22)

Due to limited time and resources, the group decided that the resistive voltage divider in figure 1.23 was the simplest and most efficient way to generate the offset voltage source. Adding too much offset would reduce the input range, therefore, a 100mV reference voltage was determined sufficient for our design. According to the resistor values in figure 10, the reference voltage is

$$V_{OFFSET} = 3.3 \left(\frac{R_{12}}{R_{11} + R_{12}} \right) = 3.3 \left(\frac{1}{1 + 32} \right) = 0.1 V \quad (15)$$

The output voltage of the AD8410A was experimentally determined to have the following relationship as a function of the voltage difference across the shunt.

$$V_{out} = 20I_{shunt}R_{shunt} + 0.1 \quad (9)$$

The output of the AD8410A is a single-ended voltage, therefore, the ADC is now configured in single-ended mode for current measurements. If 12-bit single-ended ADC measurements are made with the 2.048V reference voltage, the new voltage resolution is 0.5mV.

$$RESOLUTION = V_{min} = \frac{V_{ADCREF}}{2^{12}} = \frac{2048 \text{ mV}}{4096} = 0.5 \text{ mV} \quad (16)$$

Consequently, the smallest measurable current increment is now 0.137A and full-scale current is now 532 A (OM).

$$I_{min} = \frac{V_{min}}{A \times R_{shunt}} = \frac{0.5 \text{ mV}}{20 \times 0.183 \text{ m}\Omega} \cong \mathbf{0.137 \text{ A}} \quad (17)$$

$$I_{max} \cong \frac{V_{ADCREF} - V_{ref}}{A \times R_{shunt}} = \frac{(2048 - 100) \text{ mV}}{20 \times 0.183 \text{ m}\Omega} \cong \mathbf{532 \text{ A}} \quad (18)$$

After using the signal conditioning circuit in figure 10, the new current resolution expressed as a percentage of the full-scale value is:

$$I_{res} = \frac{I_{min}}{I_{max}} = \frac{0.137}{532} \cong \mathbf{0.0257\%} \quad (19)$$

This is a tremendous improvement compared to when a differential voltage measurement was performed on the voltage drop across the shunt without amplification. Additionally, the single-ended to differential conversion performed by the amplifier allowed us to configure the ADC in single-ended mode which has 12-bit resolution for positive unipolar input voltages. Note that the ADC is assumed to be ideal in these calculations. Inaccurate ADC measurements will not permit the current resolution to be equal to the theoretical value. Since the user interface only allows the current to be programmed with a minimum increment of 1A, the current resolution is rounded up to 1A (OM).

Current Sense Amplifier (AVR128DB48 Internal OP AMP Peripheral):

Originally, the internal OP AMP peripherals of the AVR128DB48 were configured to form an instrumentation amplifier with a gain of 15 as shown in figure 1.25 (OM).

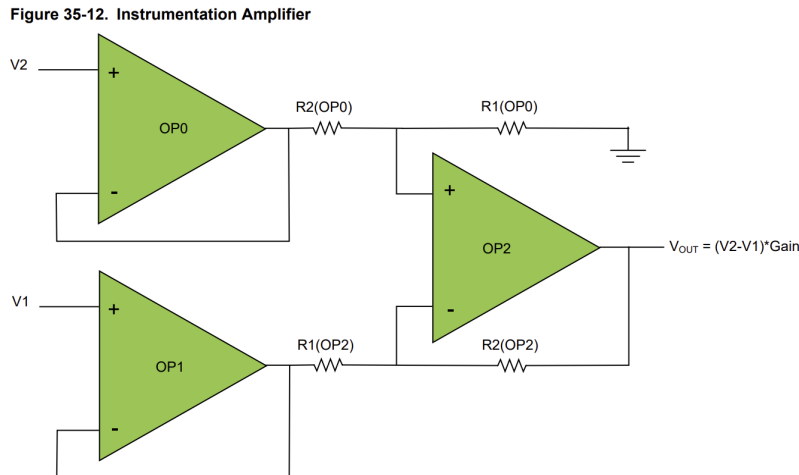


Figure 1.25: AVR128DB48 Internal OP AMPS used as Instrumentation Amplifier (Figure 35-12 of datasheet)

The first drawback is that the maximum voltage gain is limited to 15, which results in lower current resolution compared to the AD8410A with a gain of 20. However, the resolution would still remain within 1 A, and this approach reduces the need for additional external hardware, making it potentially more desirable. After programming the AVR128DB48 OP AMP peripheral to form an instrumentation amplifier with a gain of 15, the group obtained the following relationship between the input differential voltage and the gain of the instrumentation amplifier shown in figure 1.26 (OM).

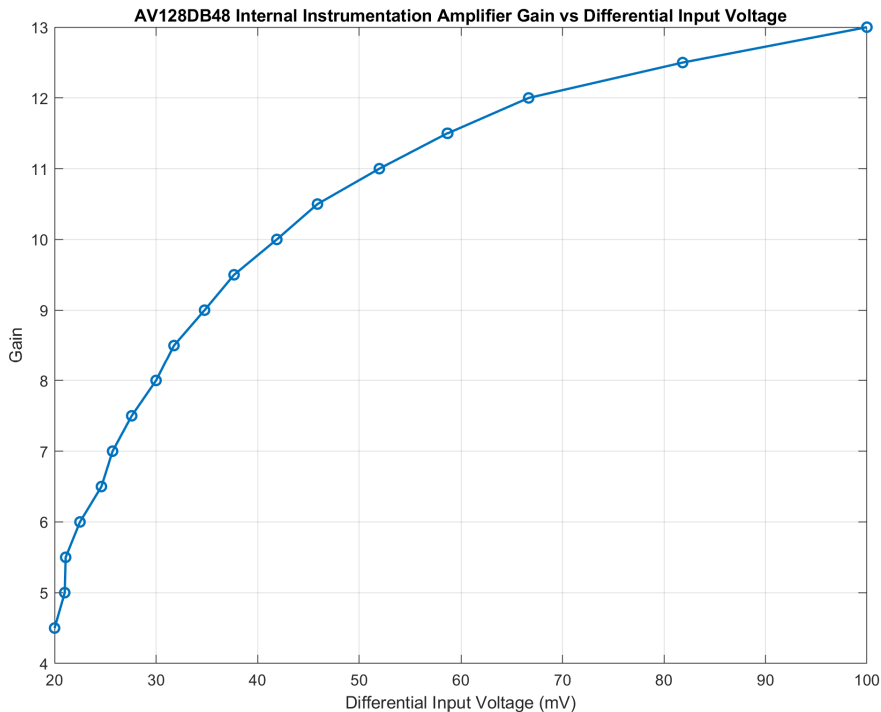


Figure 1.26: Voltage Gain vs Input Voltage for AVR128DB48 Instrumentation Amplifier (OM)

This clearly shows that the gain decreases exponentially for differential inputs below 100mV. At 500 A, the differential voltage across the shunt is only 72.5 mV, meaning that the current measurements would be highly inaccurate below 500 A.

$$V_{shunt} = I_L R_{shunt} = (500)(0.000145) = 0.0725V \quad (20)$$

This is exactly what experiments confirmed as the group was unable to measure any currents below 100 A, and even above 100 A, the measurements showed significant variability and very poor accuracy. Consequently, the team decided to use the external AD8410A as a front-end differential amplifier rather than working with the internal op amps of the microcontroller (OM).

Table 1.7 shows currents measured by the MCU and compared with the ammeter measurement. Note that the currents were set by turning the control knob manually (JL).

Table 1.7: Comparison of the MCU and Ammeter Measured Currents (JL)

Current from MCU (A)	Current from Ammeter (A)
38.6	38
100.9	100
200.4	200
340.6	340

The remote and local user interfaces only support current settings in whole-ampere increments and the currents are experimentally determined to be accurate within about 1 A. The maximum current that could be obtained from the batteries was 350 A and not 500 A as originally specified. This is due to the dynamic range of the carbon pile resistance shrinking overtime. Repeated use of the carbon pile form when it was first purchased it has resulted in the minimum resistance increasing from about 19 mΩ when first used to 37 mΩ at the time of writing. The increased series resistance limits the current drawn from the battery to about 350A. The maximum current can be increased by shaving down or removing some of the carbon disks in the stack so that their resistance is decreased (OM).

The current accuracy is determined by the precision of the AD8410A current sense amplifier and by the accuracy of the ADC. Since the output characteristic of the AD8410A with a reference offset was near ideal it is not a primary source of any current measurement inaccuracy. The current measurements are subject to the same ADC measurement inaccuracies that limit the accuracy of the battery cell voltages. Therefore, the primary source of current measurement inaccuracies is the inaccurate ADC conversions and thermal noise due to resistances (OM).

The analog ammeter calibration also influences whether the results are interpreted correctly. The scale markings on the analog ammeter only have a precision of 10 A, therefore, the group had to rely on visual judgement to interpolate in between the scale markings. This method of calibration is subject to human error as it is difficult to reliably estimate the current to within 1A of precision when the ammeter dial is in between scale markings that are 10A apart. Nevertheless, the system only allows current settings with 1 A precision, therefore, any inaccuracies less than 1 A are not significant (OM).

The current for automated tests was limited to 200 A because the torque needed to compress the carbon pile began to exceed the stepper motor's capability. As a result, the motor would get

jammed and the current would remain stuck at 200 A while the stepper motor is unable to deliver the torque necessary to rotate the knob any further. An additional feature was added to cancel the automated test and have the stepper motor open circuit the carbon pile with a pushbutton press (OM).

Section 1.6 Stepper Motor:

The carbon pile load resistance is controlled by the compression force on the carbon pile. The battery tester that the team has dismantled for its carbon pile already has a linear actuator with all of the mechanical components that are needed for this design. However, the linear actuator requires the user to manually turn a knob to adjust the force on the carbon pile and the faculty advisor would like a fully automated test that only requires a single pushbutton press. Therefore, the linear actuator that clamps down on the carbon pile needs to be electronically controlled. Since the battery tester already has a manually controlled linear actuator, the group decided to remove the knob and plug the shaft directly into a NEMA-17 stepper motor via a shaft coupler (OM).

The stepper motor can then rotate the shaft as if the user was manually rotating the knob with their hand. The team has decided to use the current reading from the shunt as feedback for the microcontroller to adjust the stepper motor position until the error between the programmed load current and the measured load current read from the shunt is minimized to within a steady-state error tolerance. A block diagram using negative feedback to electronically program the load current drawn from the battery pack is shown in figure 1.27 below (OM).

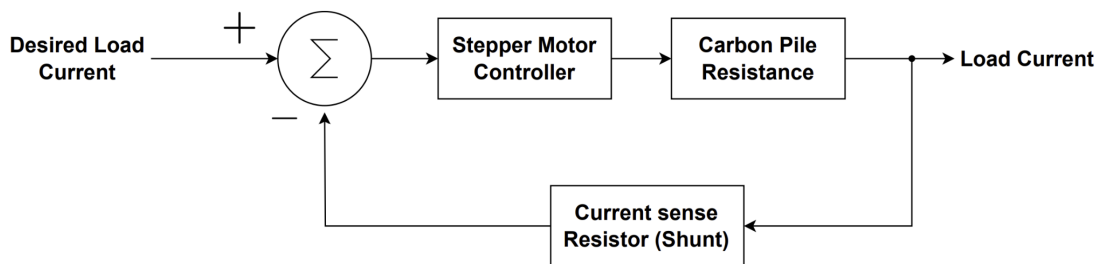


Figure 1.27: Stepper Motor Control Diagram (OM)

Additionally, an algorithmic flowchart for the software used to set the current equal to the target value is shown in figure 1.28 below:

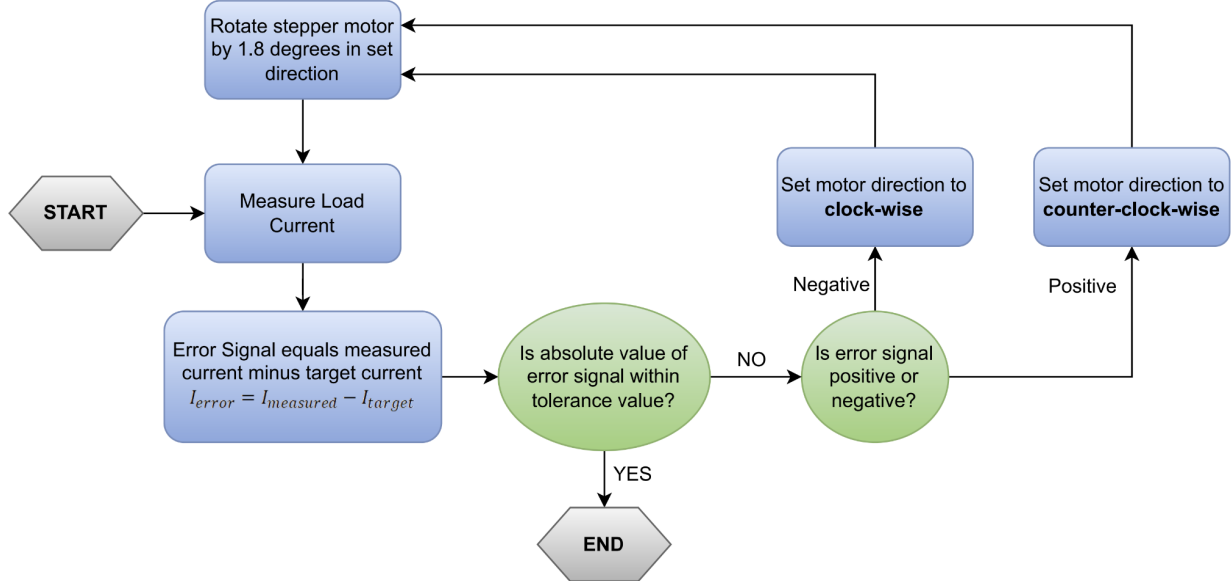


Figure 1.28: Stepper Motor Software Flowchart (OM)

The stepper motor is controlled using an A4988 driver with two MCU pins:

- One for direction control (1 = CW, 0 = CCW)
- One for generating step pulses

The A4988 is configured in full-step mode so that each step moves the motor in the set direction by 1.8 degrees. Since one full rotation is 360 degrees, 200 steps results in one full rotation. During automatic testing, the MCU uses a negative feedback loop to send STEP pulses to the motor and adjust its direction based on whether the measured load current is above or below the programmed target amount. The MCU remains in this feedback loop until the measured current level settles at the desired amount within a steady-state error tolerance. The NEMA-17 stepper motor is powered by a +12 V power supply and is currently limited to 500 mA. The group decided to use a separate carrier board to host the stepper motor driver. A image and schematic of the stepper motor board are shown in figures 1.29 and 1.30 (OM).



Figure 1.29: Stepper Motor Board on PCB (JL)

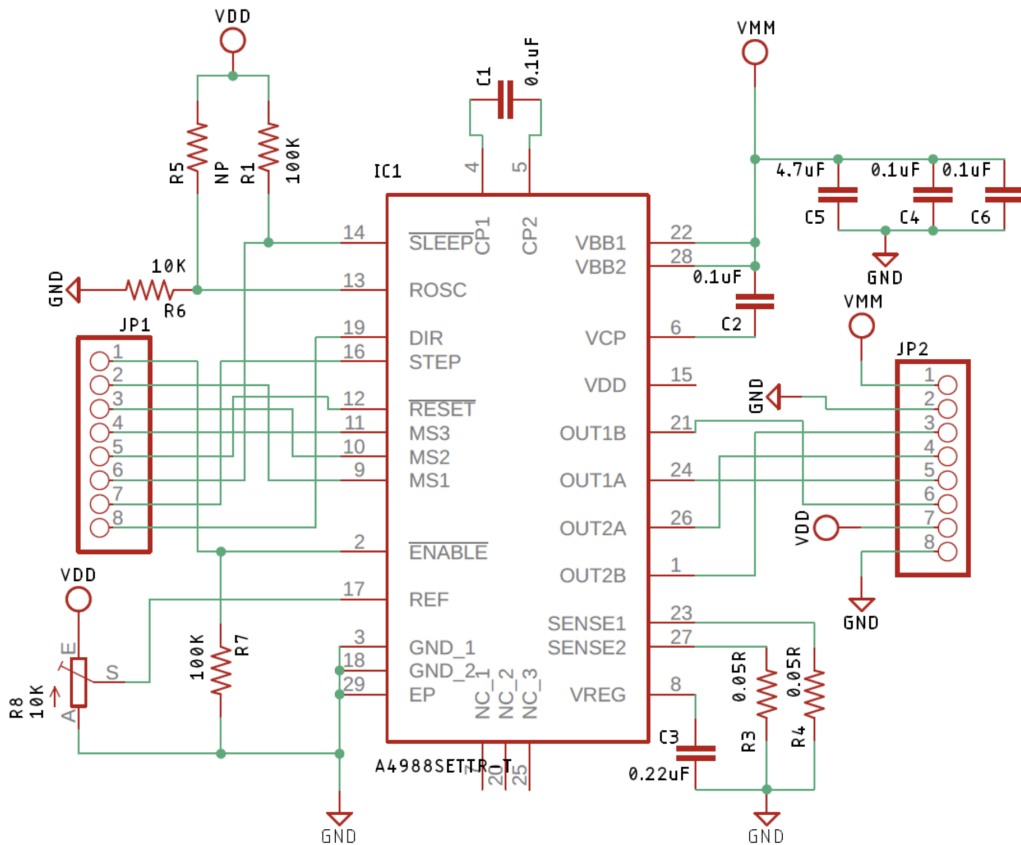


Figure 1.30: A4988 Stepper Motor Carrier Board

The stepper motor carrier board is mounted on the main PCB with female headers. The MS1, MS2, and MS3 pins are all tied to ground so that A4988 is operating in full-step mode with a step resolution of 1.8 degrees. In order to prevent the stepper motor from causing power supply ripple, a 100 uF decoupling capacitor is used to isolate the motor from the main power 12 V power supply. A 100 nF decoupling capacitor is also included to isolate the A4988 logic from the main 3.3 V power supply used to power the microcontroller. Additionally, a SLEEP control pin is connected to pin PC6 of the microcontroller in order to save power when the motor is not being used for an automated test. A schematic of the main PCB interface to the A4988 stepper motor driver board is shown below in figure 1.31 and an image of the stepper motor mechanically coupled to the carbon pile is shown in figure 1.32.

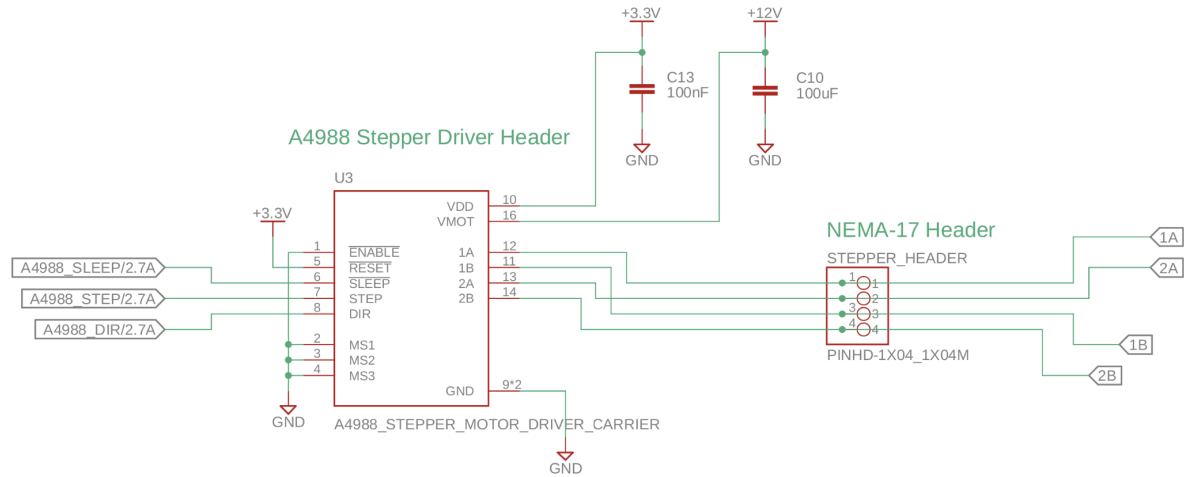


Figure 1.31: A4988 Stepper Motor Driver PCB Interface (OM)

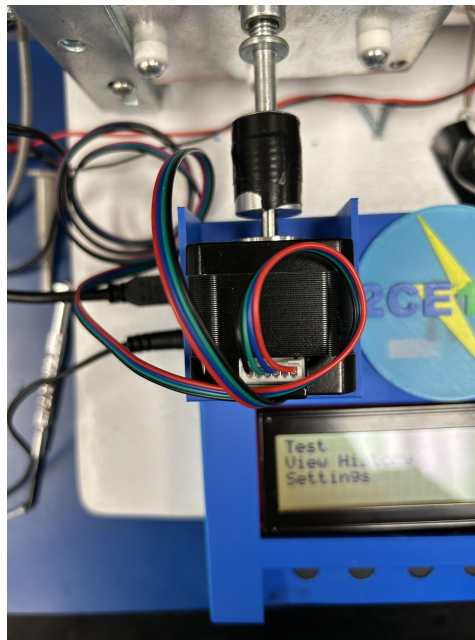


Figure 1.32: Stepper Motor Mechanical Coupling (TS)

Section 2 Local Interface Hardware:

Section 2.1 Liquid Crystal Display (LCD):

A 4 x 16 SparkFun AVR Serial Based Liquid Crystal Display (LCD) is used to display information to the user. The LCD is configured to the microcontroller using the SPI1 module, therefore, it requires SCK, MOSI, and /SS pins. MISO is not used because the LCD does not output any data. This LCD is also compatible with UART, SPI, and I2C. The group chose to use SPI, as it is generally faster than I2C and UART, allowing for quicker LCD updates. An image of the LCD and the schematic of the LCD are shown below as figures 3 and 4 respectively (JL).



Figure 2.1: LCD on PCB (JL)

LCD header

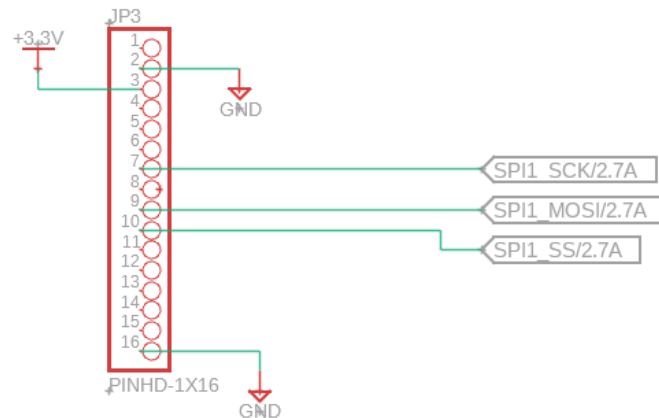


Figure 2.2: LCD Schematic (OM)

Section 2.2 Pushbuttons:

Pushbuttons are used to allow for user input while the program is running. The D6R90 F2 LFS pushbuttons are paired with decoupling capacitors to stabilize voltage fluctuations. This is a single pole single throw push button. They are pulled high normally and get pulled low when they are pressed. An image of the pushbuttons and their schematic are shown below in figures 2.3 and 2.4 respectively (JL).



Figure 2.3: Pushbuttons on PCB (JL)

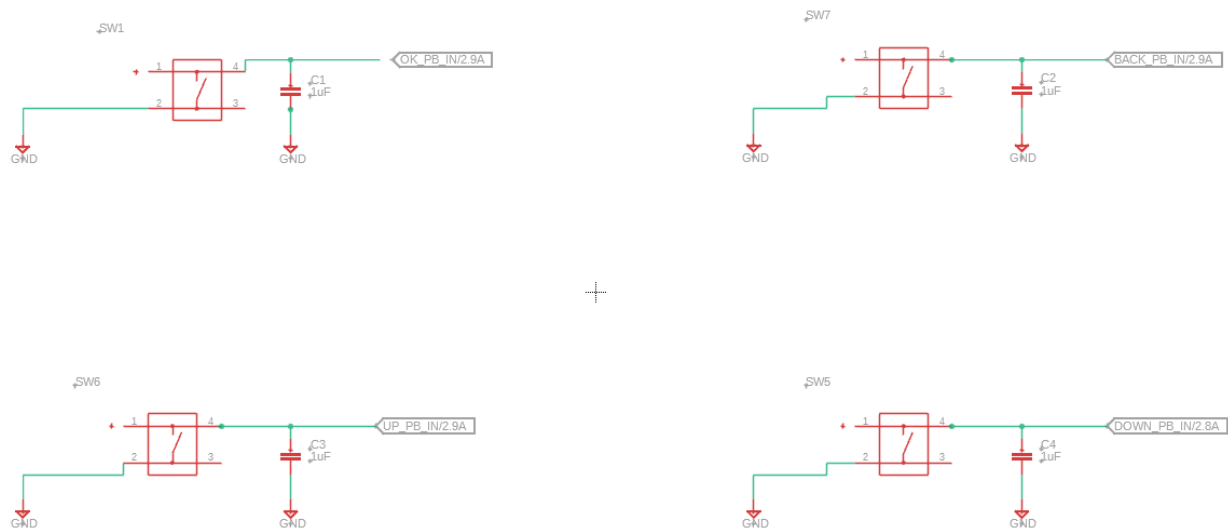


Figure 2.4: Pushbuttons Schematic (OM)

As shown in the screenshot taken from an oscilloscope in figure 2.5, there is some bounce that stabilizes in only 1.25us. This stable transition is attributed to the 1uF capacitors. Figure 2.6 shows the transient response of a single push over an extended period of time. For 81ms, the voltage across the pushbutton remains low. Then the switch opens, the voltage starts to increase back to 3.3V in 65ms. Around the 35ms mark should be sufficient for the MCU to detect a logic 1, since the lowest logic 1 is around 75% of Vdd. This results in a minimum of 115 ms of delay before the next press can be processed. We take this into account using software delays of 200ms, which should give the MCU plenty of time before each interrupt. This however, does make the local interface slower, but also ensures that presses are not accidentally triggered; for instance, this software delay prevents an automated test to start unprompted.

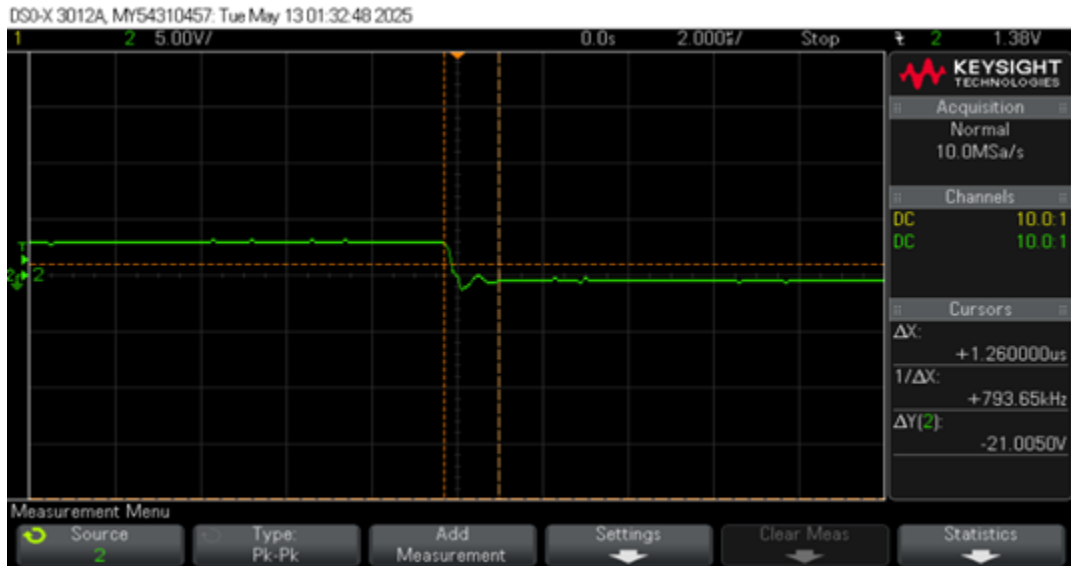


Figure 2.5: Oscilloscope Screenshot of Pushbutton Bounce (JL)

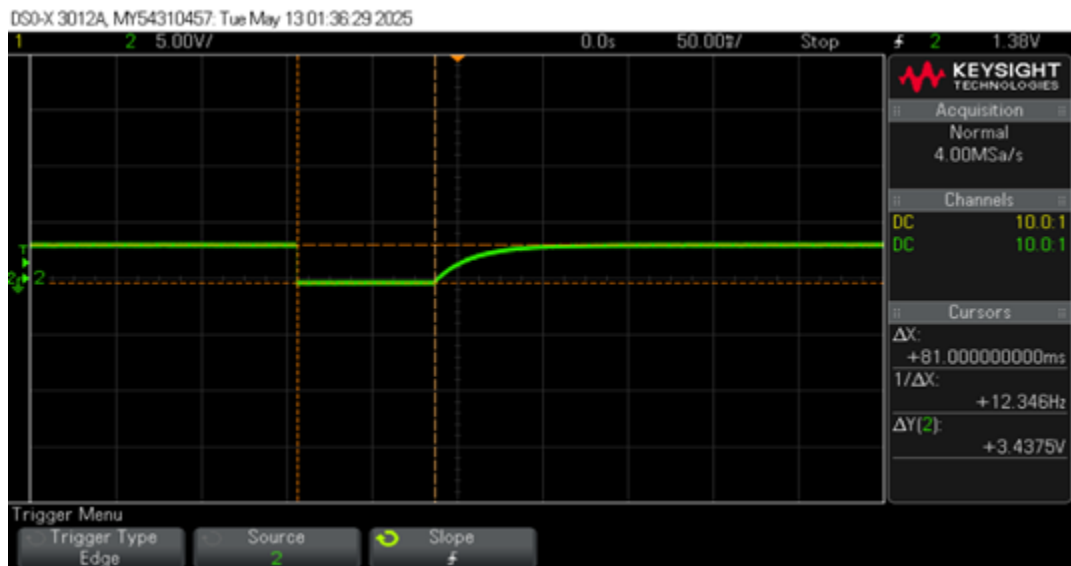


Figure 2.6: Oscilloscope Screenshot of Pushbutton Transient Response (JL)

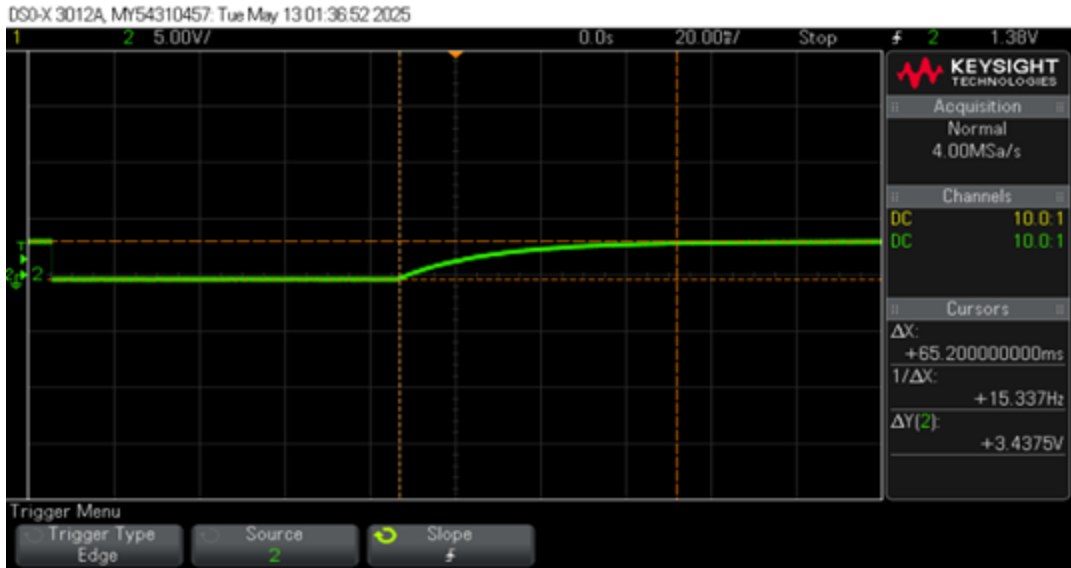


Figure 2.7: Oscilloscope Screenshot of Pushbutton Rising Voltage Time (JL)

Section 2.3 Buzzer:

A buzzer is used for audio feedback to inform the user to lower the carbon pile load current. The TDB05LFPN buzzer is used, with its positive end simply connected to pin PA5 of the microcontroller (JL). When the positive terminal is pulled high, voltage appears over the buzzer causing a loud beep. Volume can be adjusted using a potentiometer, which proved to be better than adjusting duty cycle. An image of the buzzer is shown below in figure 2.8 (JL).



Figure 2.8: Buzzer on PCB (JL)

Section 3 Remote Interface Hardware:

A block diagram of the components used in the hardware diagram is shown below in figure 3.1. The LCD, ADC, and stepper motor have all been discussed in previous sections. The only new hardware to discuss and the key component of the remote interface is the CP2102 UART Bridge (TS).

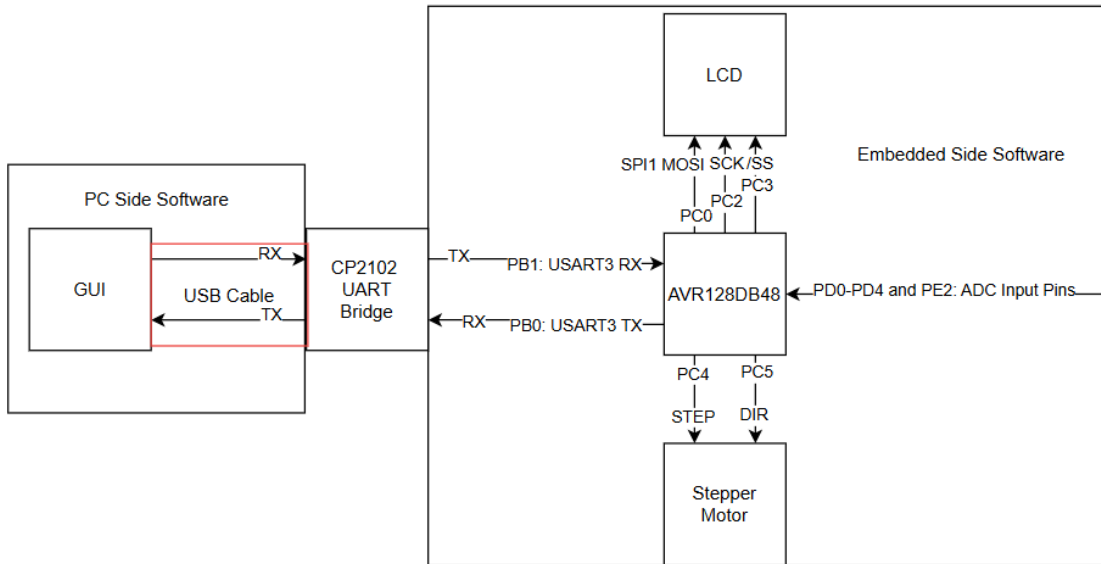


Figure 3.1: Remote Interface Block Diagram (TS)

Section 3.1 UART Bridge:

An image and schematic of the CP2102 is shown below in figures 3.2 and 3.3. The CP2102 has a micro-USB port that can be connected to the PC using a micro-USB to USB connector.

Communication is enabled using the UART protocol. The CP2102 has a 6 pin breakout board. Table 3.1 below details the pin connections and their uses (TS).

Table 3.1: Pin Connections of the CP2102 UART Bridge (TS)

Pin Number	Pin Name	Description	Connection
1	3V3	3.3 V Supplied by the CP2102	3.3 V Power Rail
2	DTR	NOT USED	NOT USED
3	RXI	Received data from the microcontroller	AVR Pin PB0 (Pin 4)
4	TXD	Transmitted data to the microcontroller	AVR Pin PB1 (Pin 5)
5	GND	Ground reference for the CP2102	GND Power Rail
6	+5V	NOT USED	NOT USED



Figure 3.2: CP2102 UART Bridge on PCB (TS)

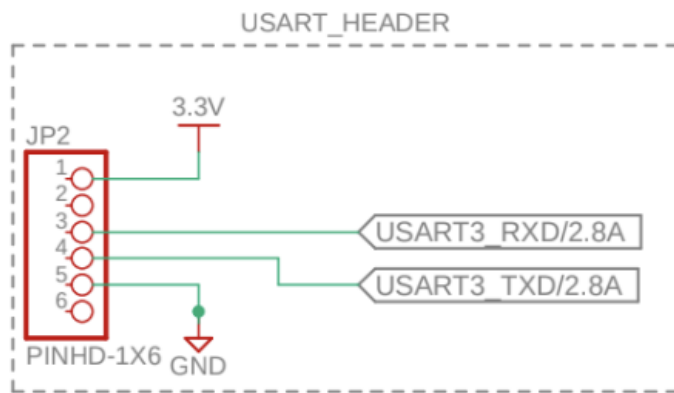


Figure 3.3: CP2102 UART Bridge Schematic (OM)

The 3.3 V and 5 V pins of the CP2102 can be used to provide power to another device. The 3.3 V pin is used in this design to power the microcontroller and other peripherals when the power supply board is not available. The 5 V pin is not used because some of the components like the LCD do not support voltages higher than 3.3 V. The TX and RX pins are flipped in that the TX pin of the CP2102 connects to the RX pin of the AVR and the RX pin of the CP2102 connects to

the TX pin of the AVR. This is done because the directions are flipped. The data transmitted by the CP2102 is received by the AVR and vice versa. USART3 is used so the TX and RX pins are PB0 (pin 4) and PB1 (pin 5) respectively. The connection of the remote interface circuitry to the microcontroller is shown in figure 3.4 (TS).

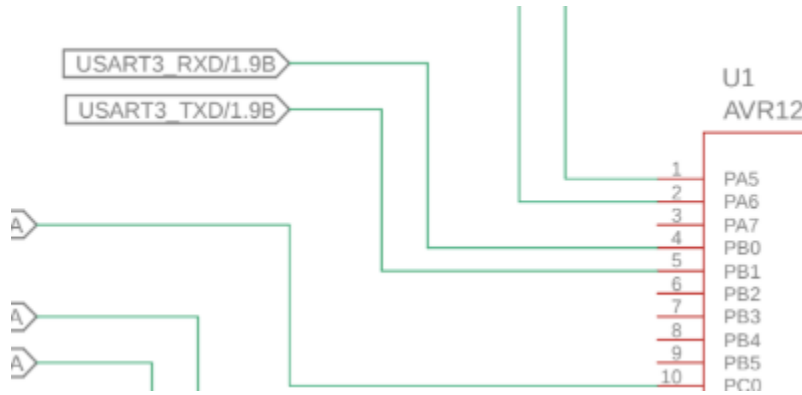


Figure 3.4: Connections from the CP2102 UART Bridge to the AVR128DB48 Microcontroller (OM)

Section 4: Other Hardware

Section 4.1: Microcontroller:

The AVR128DB48 IC is soldered onto the PCB with corresponding numberings of the pin numbers on the AVR. Images of the IC are shown below in figures 4.1 and 4.2. The chip was soldered using drag solder, and carefully inspected for shorts, as the pins are a fraction of a mm apart. Decoupling capacitors of 100nF are placed (JL).



Figure 4.1: AVR128DB48 Microcontroller on PCB (JL)

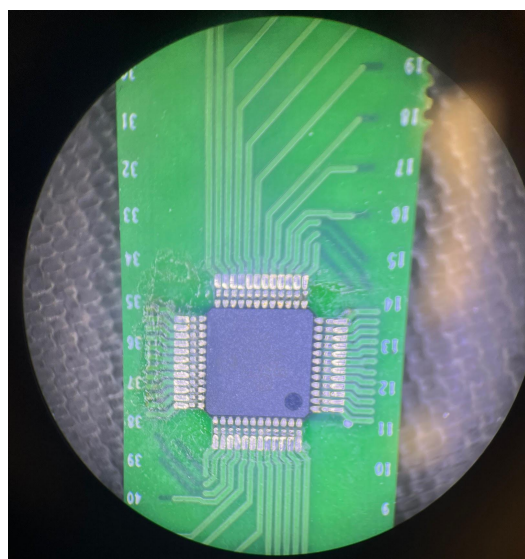


Figure 4.2: AVR128DB48 Microcontroller Under a Microscope (JL)

The schematic of the AVR is shown below in figure 4.3. Decoupling capacitors are placed between VDD and GND of the microcontroller, to act as a local energy reservoir and prevent noise and power interference. Table 4.1 below shows all of the pins of the AVR and their connections (JL).

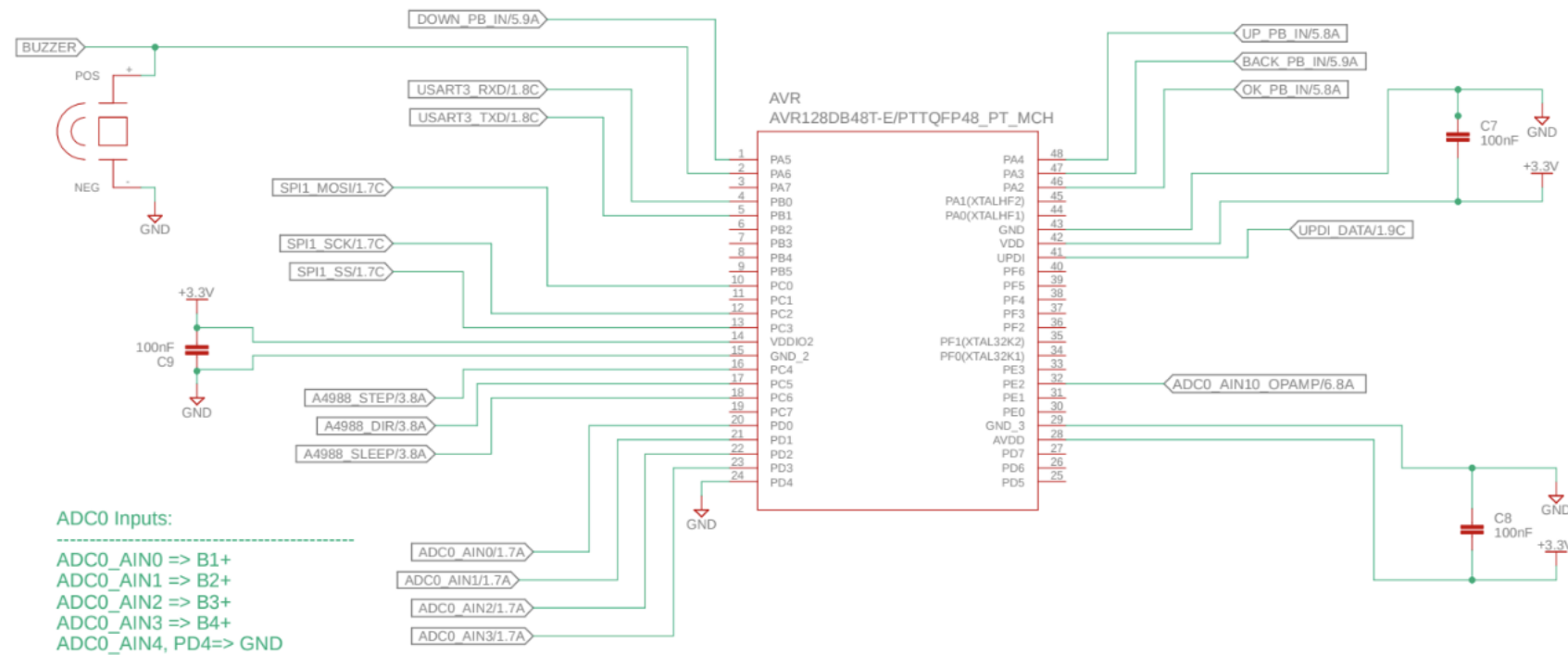


Figure 4.3: AVR128DB48 Schematic (OM)

Table 4.1: AVR128DB48 Pin Connections (JL)

Pin Number	Peripheral	Function	Board Pin Num
PA0	XTALHF1	Reserved for Clock	44
PA1	XTALHF2	Reserved for Clock	45
PA2	IO	OK PB	46
PA3	IO	BACKPB	47
PA4	IO	UP PB	48
PA5	IO	DOWN PB	1
PA6	IO	BUZZER OUTPUT	2
PA7			3
PB0	USART3_TxD	REMOTE	4
PB1	USART3_RxD	REMOTE	5
PB2			6
PB3			7
PB4			8
PB5			9
PC0	SPI1_MOSI	LCD	10
PC1	SPI1_MISO	LCD	11
PC2	SPI1_SCK	LCD	12
PC3	SPI1_SS	LCD	13
PC4	STEPPER MOTOR	A4988_STEP	16
PC5	STEPPER MOTOR	A4988_DIR	17
PC6	STEPPER MOTOR	A4988_SLEEP	18
PC7			19
PD0	ADC0_AIN0	BAT1+	20
PD1	ADC0_AIN1	BAT2+	21
PD2	ADC0_AIN2	BAT3+	22

PD3	ADC0_AIN3	BAT4+	23
PD4	ADC0_AIN4	BAT GND	24
PD5			25
PD6			26
PD7			27
PE0			30
PE1			31
PE2	ADC0_AIN10	Current Sense Input	32
PE3			33
PF0	XTAL32K1	Reserved for Clock	34
PF1	XTAL32K2	Reserved for Clock	35
PF2			36
PF3			37
PF4			38
PF5			39
PF6			40
N/A	VDDIO2	Power Supply	14
N/A	GND	Power Supply	15
N/A	AVDD	Power Supply	28
N/A	GND	Power Supply	29
N/A	UPDI	Programming Microcontroller	41
N/A	VDD	Power Supply	42
N/A	GND	Power Supply	43

Section 4.2: JTAG ICE Programmer:

The provided AVR128DB48 microcontroller does not have a built-in programmer. Therefore, a separate programmer is needed to program the microcontroller with new instructions. The JTAG ICE programmer was chosen as the external programming device. An image of the JTAG ICE Programmer is shown below in figure 4.4.



Figure 4.4: JTAG ICE External Programmer (TS)

This device has a 10 pin header. The pin connections and their uses are provided below in table 4.2. A schematic of the pin connections are provided below in figure 4.5 (TS).

Table 4.2: Pin Connections of the JTAG ICE 10 Pin Header (TS)

Pin Number	Pin Name	Description	Connection
1	TCK	NOT USED	NOT USED
2	GND	The ground reference to power the ICE	GND Power Rail
3	TDO	Transmits data to the microcontroller to be programmed	AVR UPDI (Pin 41)
4	VTG	The VDD to power the ICE	3.3 V Power Rail
5	TMS	NOT USED	NOT USED
6	/RST	NOT USED	NOT USED
7	NONE	NOT USED	NOT USED
8	NONE	NOT USED	NOT USED
9	TDI	NOT USED	NOT USED
10	GND	NOT USED	NOT USED

male JTAG Programming Header

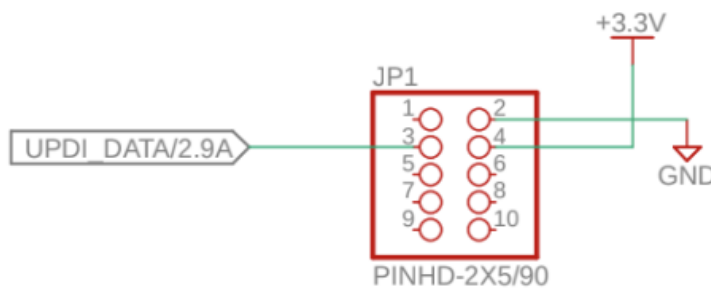


Figure 4.5: JTAG ICE 10 Pin Header Schematic (OM)

The ICE JTAG needs power from the power supply board to operate. This is provided by the 3.3 V and GND connections on pins 2 and 4. Pin 3 (TDO) is the UPDI pin that programs the

microcontroller. It is connected to the UPDI pin of the AVR128DB48 (pin 41) as shown below in figure 4.6. The PCB header connection is shown below in figure 4.7. No other pins of the header are used in this design (TS).

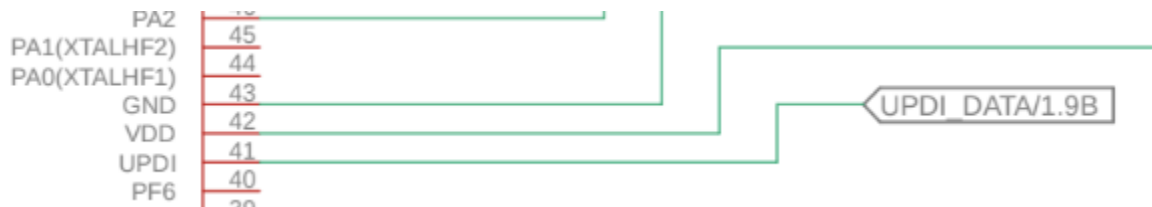


Figure 4.6: Connections from the JTAG ICE 10 Pin Header External Programmer to the AVR128DB48 Microcontroller (OM)



Figure 4.7: PCB JTAG Header Connection on PCB (JL)

Section 4.3 Power Supply Board:

The power supply board is shown below in figures 4.8 and 4.9. It uses the LM2596 buck converter. The schematic is shown below in figure 4.10. R2 is the upper resistance of the potentiometer and R1 is the resistance of the lower half of the potentiometer. The potentiometer is used to adjust the output voltage. This power supply is used to generate 3.3V for the circuit, and two additional wires from the 12V line will be used to power the fan and stepper motor. A switch is used to turn the power to the board on and off (JL).



Figure 4.8: Power Supply Board on Front Side of PCB (JL)



Figure 4.9: Power Supply Board on Back Side of PCB (JL)

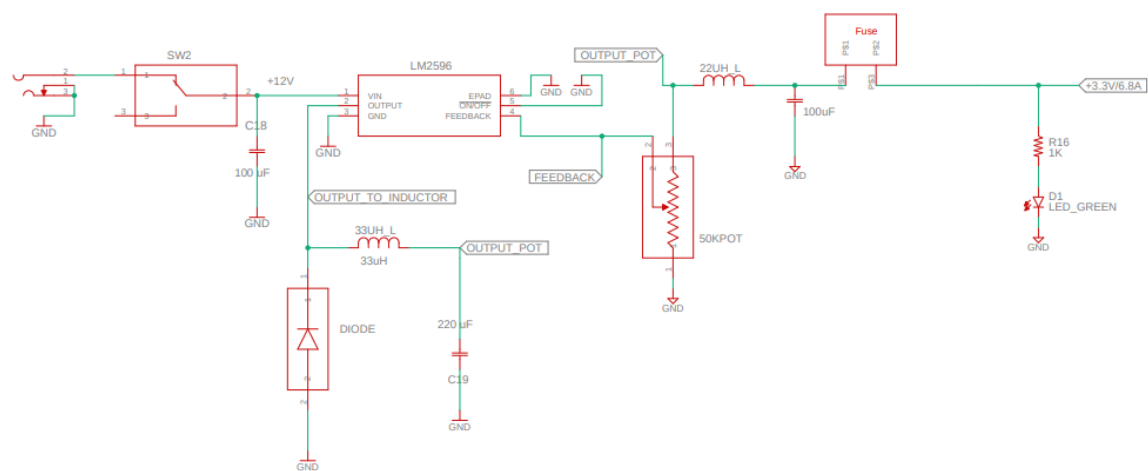


Figure 4.10: Power Supply Board Schematic (JL)

In figure 4.8 above, the red box indicates the DC barrel power jack connector, which is used to receive 12V and transfer it to a switch. The single pole single throw (SPST) switch controls the power to the buck converter circuit, allowing the entire system to be turned on or off.

A simple buck converter circuit using the LM2596 (highlighted in purple on the back of the board) is implemented, with a variable output controlled by a potentiometer connected as part of the feedback loop. The rest of the circuit is boxed in orange. The inductor and capacitor values were carefully selected to filter noise and smooth the PWM signal produced by the buck converter. This converter operates at 150 kHz, with an input voltage range of up to 40V and an output range of 1.23V to 37V.

The equation governing the output voltage based on the feedback resistance is:

$$V_{out} = V_{ref} \times (1 + R_2/R_1) \quad (21)$$

In this implementation, R1 and R2 are formed by the adjustable potentiometer.

Using the external power supply board, presented no issues except that the LCD occasionally displayed black boxes, likely due to noise in the output voltage. To address this, an additional inductor-capacitor filter was added to provide a more stable voltage to the onboard power supply.

Initially, however, the output remained at a constant 12V, regardless of the potentiometer's wiper position. This issue occurred because the original 50k Ω potentiometer created too high of an impedance in the feedback network, preventing the LM2596 from receiving a stable feedback voltage. As a result, the converter defaulted to its maximum duty cycle, outputting nearly the full input voltage. Replacing the potentiometer with a 10k Ω version provided a more suitable feedback divider, allowing the output voltage to be adjusted as expected.

However, due to the light-load behavior of the buck converter, the output was still unstable at lower voltages. Adding a small load, such as a status LED, helped stabilize the output and enabled the full voltage adjustment range (from 1.23V to ~11.9V). This improvement occurred because the load helped dissipate stored energy in the output capacitor and reduced output ringing.

The potentiometer is currently secured with hot glue to prevent accidental movement of the wiper, which could cause the output voltage to rise unintentionally. Although through-hole resistors could replace the potentiometer for fixed voltage, we chose not to desolder it to avoid damaging nearby components with hot air rework, especially after having removed and replaced several parts during troubleshooting.

Finally, a fuse is placed in series at the output to the rest of the circuit and is marked with a yellow box. The fuse was rated for 1A, meaning if the MCU or other components draw more than 1A, the fuse will blow to prevent damage. However, the fuse is not essential in this circuit, since the battery sensing voltages are isolated from the main power rail, and the fan and motor 12V lines are also isolated from the MCU's power supply. For now, the two through-holes for the fuse are bridged, effectively shorting them. Installing a fuse remains optional depending on the application.

Table 4.3 shows the performance of the power supply circuit with different input voltages and resistances (JL).

Table 4.3: Power Supply Circuit Performance with Different Input Voltages and Resistances (JL)

Vin (V)	R2 (ohms)	R1 (ohms)	Expected Vout (V)	Vout (V)	% Error
4	3047	1903	3.21	3.3	2.8
4	1321	3629	1.67	1.71	2.4
4	0	4950	1.23	1.65	3.4
4	4850	100	4	3.85	3.75
5	4850	100	5	4.82	3.6
6	4850	100	6	5.78	3.7
8	4109	841	7.34	7.6	3.5
20	4850	100	20	19.45	2.75
20	3047	1903	3.21	3.3	2.8